Hindawi
Adsorption Science & Technology
Volume 2022, Article ID 6454354, 16 pages
https://doi.org/10.1155/2022/6454354

Research Article

Simple Preparation of the CuO•Fe_3O_4/Silica Composite from Rice Husk for Enhancing Fenton-Like Catalytic Degradation of Tartrazine in a Wide pH Range

Khanh Huyen Pham Ngoc and Anh-Tuan Vu

School of Chemical Engineering, Hanoi University of Science and Technology, Vietnam

Correspondence should be addressed to Anh-Tuan Vu; tuan.vuanh@hust.edu.vn

Received 2 March 2022; Revised 6 May 2022; Accepted 18 May 2022; Published 16 June 2022

Academic Editor: Mehdi Vosoughi

SiO_2 was prepared from rice husk (RH) with the assistance of cetrimonium bromide (CTAB), and the CuO•Fe_3O_4/SiO_2 composite was prepared by a simple coprecipitation method to enhance the Fenton-like degradation of dyes in a wide pH range. SiO_2 was a mesoporous material with a relatively large surface area of 496.4 m^2/g and a highly relative pore volume of 1.154 cm^3/g. The Fe_3O_4 and CuO particles with the size of 20–50 nm were well dispersed in the composite, making the composite tighter and causing the disappearance of large pores in the range of 20–55 nm. The surface area and pore volume of the composite were reduced to 248.6 m^2/g and 0.420 cm^3/g, respectively. Fe_3O_4/SiO_2 and Fe_3O_4 samples only exhibited high catalytic activity in an acidic medium, while the CuO•Fe_3O_4/SiO_2 composite could effectively work in a wide pH range of 3–7. Besides, the effects of reaction conditions such as catalyst dosage, H_2O_2 concentration, and initial dye concentration on the catalytic performance of the composite were studied. The optimal conditions for the degradation of dye were tartrazine (TA) concentration of 50 mg/L, dosage catalyst of 0.5 g/L, H_2O_2 concentration of 120 mM, and pH 5. The CuO•Fe_3O_4/SiO_2 composite reached the highest activity at pH 5, showing a degradation efficiency (DE) of 93.3% and a reaction rate of 0.061 min^{-1}. The reusability of the catalyst was investigated by cyclic experiments. The DE of the 3rd reuse remained at 55.1%, equivalent to 93.5% of the first use. The catalytic mechanism for the Fenton system has also been proposed.

1. Introduction

The rice husk is obtained from the milling of rice. It is a huge source of silica raw material that is discharged into the environment every year. Currently, the annual production of rice in the world is estimated at 700 million tons. RH contains about 20% of the weight of rice; its composition includes cellulose (50%), lignin (25%–30%), silica (15%–20%), and moisture (10%–15%) [1]. Vietnam is one of the leading rice-exporting countries in the world [2]; the annual rice production is 37 million tons, equivalent to 7.4 million tons of RH discarded annually. It could be used as fuel, water filter, rice husk firewood, biogas product, construction materials, and activated carbon product [3, 4]. An alternative, using RH to create highly functional silica, is an attractive research to scientists. Many shapes of silica have been made from RH such as spheres, rods, and plates for applications in construction, environment, energy storage, and catalyst [3, 5–7], where the mesoporous silica and its composite have been proven as an effective material in the adsorption and degradation of organic substances in wastewater due to its high surface area, good thermal stability, and favorable hydrothermal stability [8].

The rapid development of industry, agriculture, and services in developing countries leads to a large amount of wastewater being discharged into the environment every year [8]. Water sources are seriously polluted from wastewater causing serious impacts on ecosystems and human health. One of the typical toxic organic substances is the dye used in textiles, leather, cosmetics, printing, paper, and paint in industries [9]. The dye is the most widely used for dyeing acrylic fibers, which ionize in an aqueous solution

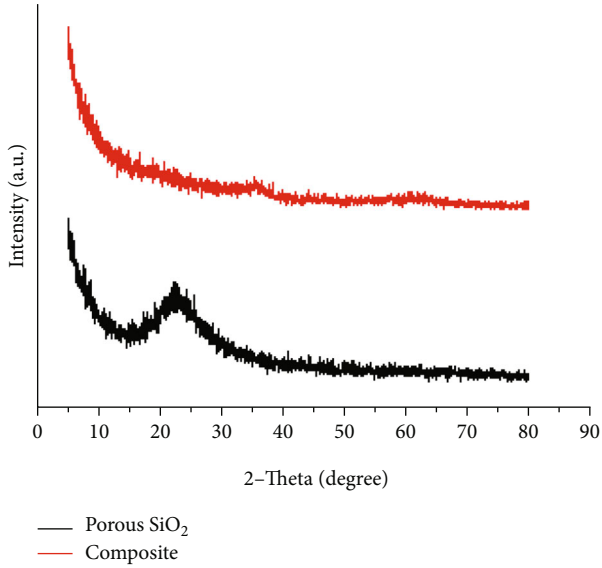

FIGURE 1: XRD patterns of porous SiO_2 and CuO•Fe_3O_4/SiO_2 composite.

and produce colored cations [10]. Dyes have a complex structure that is often stable and resistant to biodegradation [11]. There are more than 10000 different commercial dyes used in the textile process; approximately 15% of the total production is lost as wastewater during dyeing processes [12]. Intermediate products from the degradation of dyes are considered to be a major health hazard to the environment, humans, and other organisms, especially aquatic organisms [13]. Therefore, toxic and persistent organic substances in wastewater need to be removed before being discharged into the environment. There are many methods of removing organic pollutants that have been reported [14–18].

TA is an azo dye with a characteristic –N=N– bond [19]. Foods containing too high concentrations of TA will lead to human health hazards such as allergies and asthma, affect the nervous system, and more seriously increase the risk of death. According to international standards, the amount of TA allowed for human consumption is 7.5 mg/kg bodyweight/day, in nonalcoholic beverages; TA should not exceed 0.01 g/mL [20, 21]. Nowadays, conventional treatment procedures are inadequate and disabled for handling the highly persistent hazardous materials; experiments are still being conducted to create a more effective method [22].

Typical researches on the electrolysis process for treatment of dyes were the electroactive persulfate process from aqueous solutions for removal of basic Violet 16 [6] and the anodic oxidation process with graphite anode coated with lead dioxide for degradation of methylene blue and real textile wastewater [9]. Photocatalysis showed to be an effective catalyst to remove dyes under irradiation. ZnO could remove phenol under UV-C light [22], nano zerovalent iron (nZVI) can degrade acid red 14 under UV-C light in the presence of H_2O_2 and persulfate ($S_2O_8^{2-}$) [23], copper oxide nanoparticles showed high activity with metronidazole antibiotic under UV light [24], and persulfate activated by UV and ferrous ions could decompose dimethyl phthalate [25]. Adsorption was an efficient process for materials with a large surface area and easy recovery such as clinoptilolite zeolite [11], activated carbon [26], carbon nanotubes modified by nZVI [27], mesoporous magnetite/zeolite nanocomposite [28], $Fe^{II}Fe_2^{III}O_4$@GO [29], Fe_3O_4/GO [30], iron oxide/carbon nanocomposite [31], and magnetic chitosan/graphene oxide [32]. These materials are currently effective adsorbents for removing basic violet, methylene blue, nitrate, dimethyl phthalate, diphenyl phthalate, 2,4-dinitrophenol, lead, and fluoride. Other methods to enhance the removal of organic compounds in wastewater could be done by adding H_2O_2 to the decomposition process [33–35].

AOPs have been reported as promising technologies for the elimination of organic pollutants due to their high performance, simple operation, and inexpensive material [36] since AOPs were based on the generation of highly oxidizing radicals (hydroxyl radicals $OH^{\bullet}$, hydroperoxyl radicals $HO_2^{\bullet}$, and superoxide radicals $^{\bullet}O^{2-}$) to degrade organic compounds into CO_2, H_2O, and inorganic ions [37]. Also, photocatalysts and Fenton catalysts have proven to be highly effective in the aqueous medium and are suitable for applications in industrial wastewater treatment [1, 38–40].

Fenton catalysts with iron valences of 0, II, and III on silica-based materials were effective catalytic systems for oxidizing toxic and persistent organic substances. The Fe_2O_3•SiO_2 composite was synthesized by the impregnation method for degrading tartrazine at 60 mg/L, and the degradation efficiency reached 98.5% in 80 min [1]. Interactive nanospheres in the Fe_2O_3/SiO_2 composite synthesized by the emulsion method could improve the catalytic performance, and the degradation efficiency of methylene blue approached 88% in 80 min [41]. The thin slice of iron-mesoporous silica prepared by ball milling followed by uniaxial pressing and calcination could adsorb and degrade methylene blue at efficient removal of 99.94% at the concentration of 1000 mg/L [42]. A mesoporous α-Fe_2O_3/SiO_2 composite with a highly ordered mesostructure showed a high adsorption capacity of 90 mg/g and superior heterogeneous Fenton-like catalytic activity for removal of methylene blue; the removal efficiency was 100% at the concentration of 300 mg [43]. SiO_2-encapsulated zero-valent iron nanoparticles were prepared for degradation of methylene blue; the degradation efficiency was 94.2% at the ethylene concentration of 16 mg/g [44]. However, these Fenton catalytic systems remained with some drawbacks including the difficulty of catalyst recovery, cost-intensive sludge processing, and disposal process, which limited working in the low pH range (pH < 3) [45–47]. This will create difficulties to adjusting the pH for the catalysis process and neutralizing the treated wastewater before being discharged into the environment.

Magnetic particles are commonly used for the Fenton process because they are easily separated from the solution by magnets after the reaction. In addition, Fe_3O_4 has the super magnetic property and both of Fe (II) and Fe (III) irons could activate H_2O_2 to produce strong oxidizing radicals that could enhance its catalytic ability [48, 49]. Moreover, the catalyst activity of Fe_3O_4 could also be improved

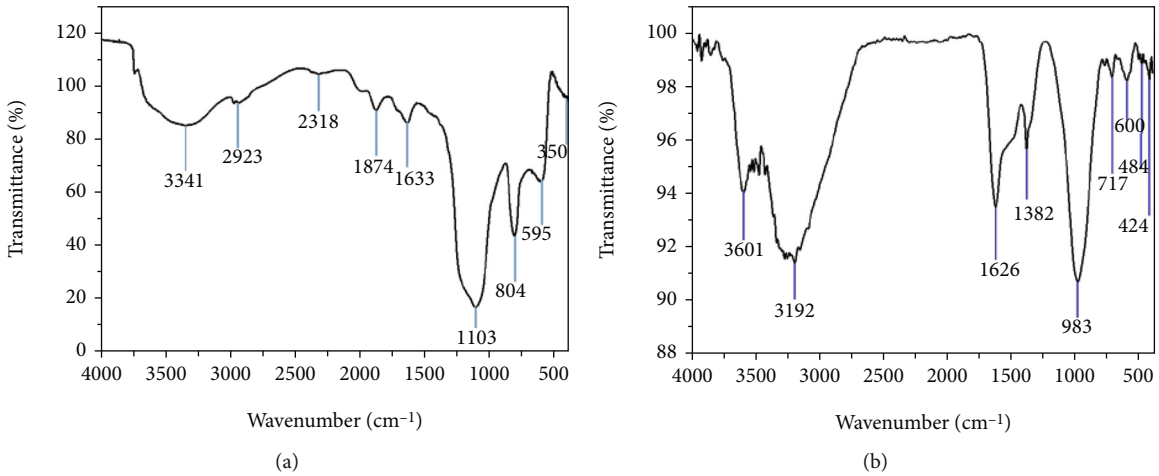

Figure 2: FT-IR spectra of (a) SiO_2 and (b) $CuO{\bullet}Fe_3O_4/SiO_2$ composite.

by combining it with noble metals [50–52] and transition metal oxides [53–55]. Surface interactions between metal oxide phases, crystal structure, phase structure, and synergistic interactions between components could be the causes for the enhanced catalytic ability in the wide pH range.

In this study, SiO_2 was prepared from rice husk (RH) with the assistance of CTAB and the $CuO{\bullet}Fe_3O_4/SiO_2$ composite was prepared by simple coprecipitation method to enhance the Fenton-like degradation of dyes in a wide range of pH in solution. As-prepared samples were characterized by XRD, N_2 adsorption/desorption isotherm, FT-IR, FE-SEM, EDS, and TEM. The catalytic performance of samples was evaluated by the oxidation of tartrazine (TA) in the presence of H_2O_2. The effects of reaction conditions such as pH, H_2O_2 concentration, catalytic dosage, and initial TA concentration on the degradation of TA were carried out. The degradation kinetics were obtained from fitting the experimental profile with time by using the first-order kinetic model. Additionally, the reusability of catalyst was evaluated by cyclic experiment.

2. Materials and Method

2.1. Materials. Rice husk was obtained from a farm in Thai Binh province of Vietnam, the silica content was determined by mass analysis, and the result showed that rice husk contained 21.3 wt.% of silica. Cetrimonium bromide (CTAB) (99.0%), copper nitrate trihydrate ($Cu(NO_3)_2.3H_2O$) (99.0%), iron(II) sulfate heptahydrate ($FeSO_4.7H_2O$) (99.0%), iron(III) chloride hexahydrate ($FeCl_3.6H_2O$ 99.0%), NaOH (99.0%), HCl (99.0%), and hydro peroxide (H_2O_2 99.0%) were obtained from Merck. Tartrazine (99%) was purchased from Sigma-Aldrich.

2.2. Synthesis of Porous SiO_2. The synthesis of silica was modified from the previous report with the assistance of CTAB [56]. Typically, RH is removed from the soil with distilled water and then soaked in 0.5 M HCl for 30 minutes to remove metal impurities. After washing with distilled water to reach pH~7, RH was dried at 100°C for 24 h. Dry RH was then burned at 600°C under airflow for 2 h to obtain rice husk ash (RHA). Subsequently, 5 g of RHA was added to an Erlenmeyer flask with 100 mL of 2 M NaOH; the mixture was heated and stirred continuously for 2 h to dissolve the silica from the ash. After cooling, the solution was filtered to remove the residues and obtain sodium silicate.

Porous SiO_2 was prepared from sodium silicate by the hydrothermal method. In a typical experiment, 40 mL of abovementioned sodium silicate was added into the mixture of 2.187 g of CTAB and 34 mL of 0.6 M HCl under stirring for 1 h; pH was controlled as 7.5–8.5 by using 6 M HCl. The mixture was aged at 50°C for 24 h. Subsequently, the white gel was transferred into an autoclave and heated up to 100°C for 48 h. The precipitate was washed with distilled water to remove surfactants and acids until neutral. The white solid was dried at 100°C for 12 h before heating at 600°C for 6 h to obtain SiO_2 powder.

2.3. Synthesis of the Porous $CuO{\bullet}Fe_3O_4/SiO_2$ Composite. The porous $CuO{\bullet}Fe_3O_4/SiO_2$ composite was prepared by the simple coprecipitation method. Typically, 2.156 g of $FeSO_4.7H_2O$, 4.197 g of $FeCl_3.6H_2O$, and 0.6655 g of $Cu(NO_3).3H_2O$ were added into a beaker containing 200 mL of distilled water under stirring for 20 min; 0.2 g of SiO_2 was then added into the mixture. The pH of the mixture was adjusted to 10.0 by using 3 N NaOH solution and stirred at 60°C for 3 h to form the dark gel. The solid gel was carefully washed several times by distilled water and ethanol and then dried at 60°C at 12 h in an oven to obtain dark powder $CuO{\bullet}Fe_3O_4/SiO_2$ composite.

2.4. Characterization. The crystalline phase of samples was investigated by X-ray powder diffraction. XRD patterns were obtained by using a Bruker D8 Advance diffractometer (Germany) with Cu Kα irradiation (40 kV, 40 mA). The 2θ ranging from 20 to 80° was selected to analyze the crystal structure. The morphology and size of the samples were observed by transmission electron microscopy (TEM, JEM-2010) and the emission scanning electron microscopy (FE-SEM, JEOL-7600F). The textural properties were measured

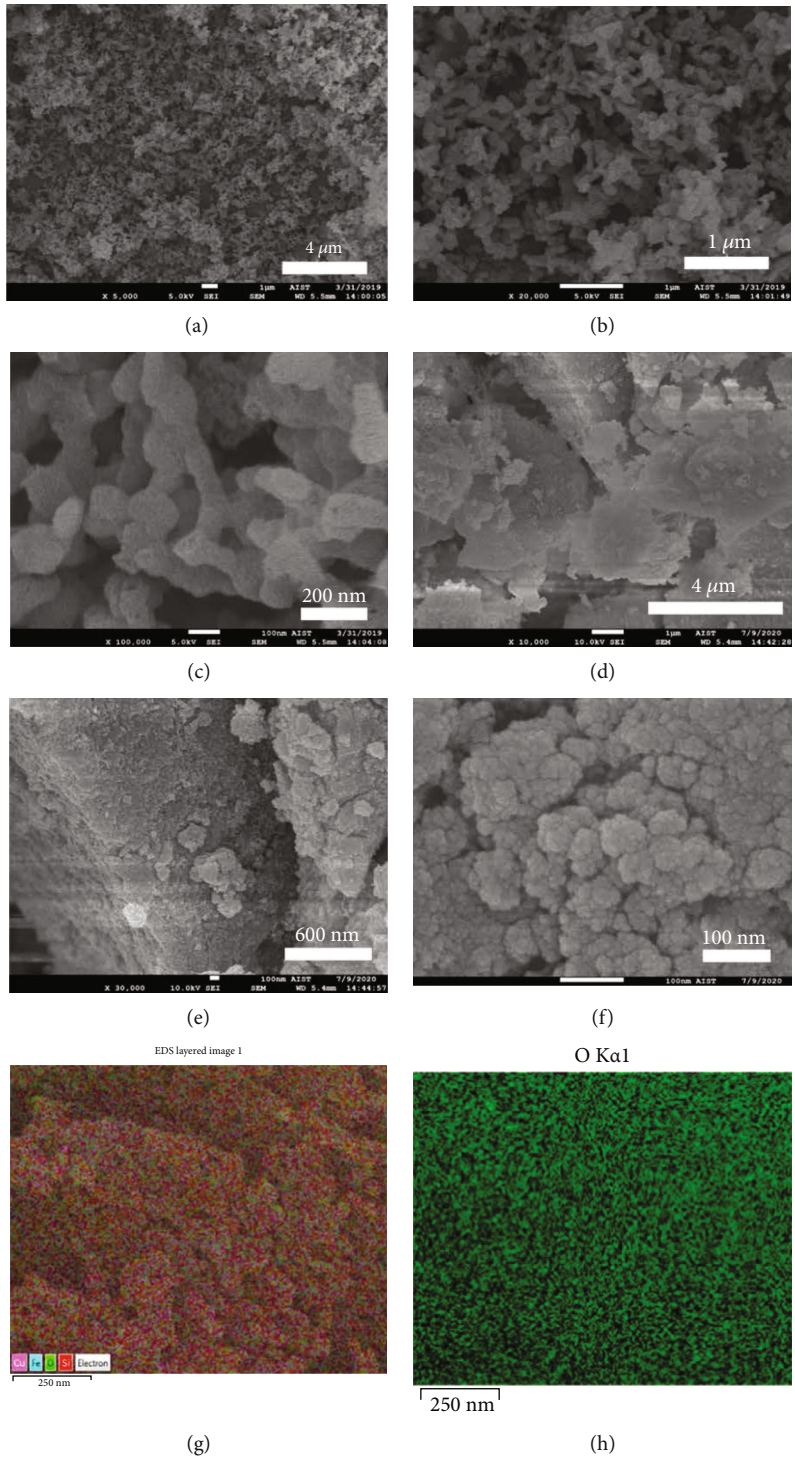

Figure 3: Continued.

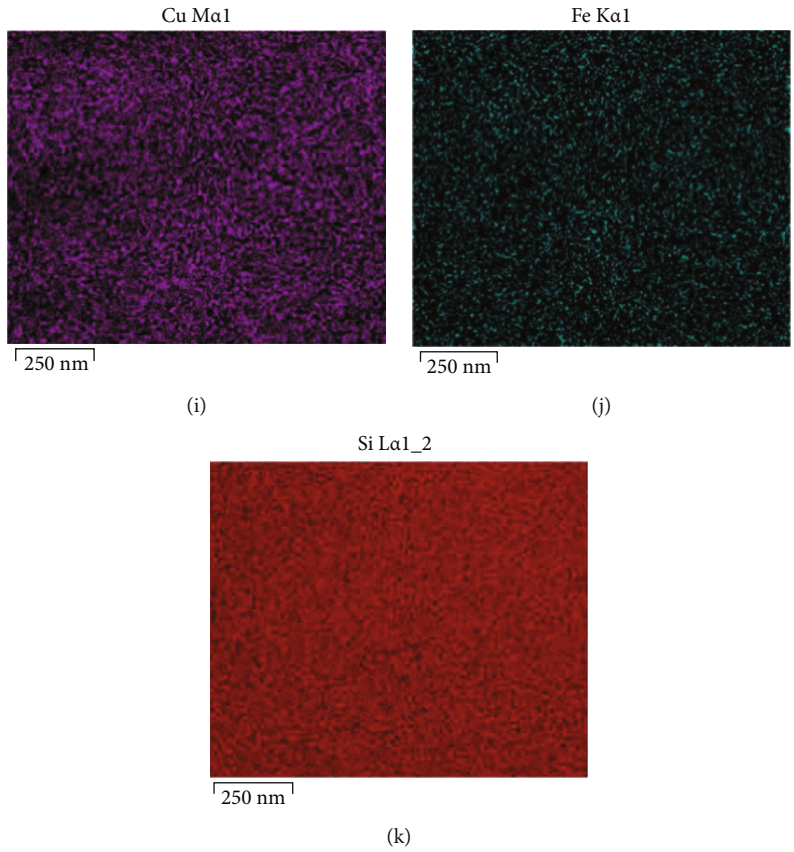

FIGURE 3: (a) FE-SEM images of SiO_2, (d–f) FE-SEM images and (g) EDS image of CuO•Fe_3O_4/SiO_2 composite, (h) O elemental map, (i) Cu elemental map, (j) Fe elemental map, and (k) Si elemental map of CuO•Fe_3O_4/SiO_2 composite.

via N_2 adsorption/desorption isotherms using micromeritics (Gemini VII). The specific surface area was obtained by using the Brunauer-Emmett-Teller (BET) method; the pore volume and pore diameter were determined by the Barrett, Joyner, and Halenda (BJH) method.

2.5. Fenton-Like Catalyst Test. The batch test was used to evaluate the TA degradation efficiency of the prepared catalyst. 50 mg of the catalyst was added to 100 mL of the dye solution and a certain amount of H_2O_2. The pH of the solution was adjusted by adding 0.1 M HCl or 0.1 M NaOH. At different time intervals, approximately 2 mL of the mixture was withdrawn and filtered using a syringe filter (0.45 μm PTFE membrane). The dye concentration was analyzed using a UV-vis spectrophotometer (Agilent 8453) at 426 nm. The degradation efficiency (DE) and rate constant (k_{ap}) of TA in the catalyst were calculated by equations (1) and (2) as follows:

$$\mathrm{DE}\,(\%) = \frac{C_{0-}C_t}{C_0} \times 100\%, \quad (1)$$

$$\ln \frac{C_0}{C_t} = k_{ap} \times t \quad (2)$$

where k_{ap} (s^{-1}) is the rate constant, C_0 is the initial concentration of TA, C_t is the concentration of TA in time, and t is reaction time presented by min and s for equations (1) and (2), respectively.

3. Results and Discussion

3.1. Characterization. The X-ray diffraction patterns of SiO_2 and the CuO•Fe_3O_4/SiO_2 composite are shown in Figure 1. The peak at 2θ of 22.8° was attributed to the amorphous silica [57]. The XRD analysis of the composite was relatively different from SiO_2. The diffraction peak of SiO_2 almost disappeared in the composite. The low-intensity peaks at 2θ of 35.6 and 62.2° could be assigned to Fe_3O_4 (PDF#88-0886) [58]. There were no signals of CuO observed for the composite. However, the composition of the metals in the composite is shown in the EDS result below. This result implied that Fe_3O_4 and CuO oxides were formed only at low crystallinity after the synthesis process by salts and with a short aging time.

FT-IR transmittance spectra of SiO_2 and the CuO•Fe_3O_4/SiO_2 composite are presented in Figure 2. For observation of SiO_2, the broad peak from 3000–3700 cm^{-1} was assigned to the presence of O-H stretching vibration of Si-O-H and adsorbed water (H-O-H) [1]; the peak at 1633 cm^{-1} could be attributed to the vibration bending of O-H. The intense bands at 1103, 804, and 595 cm^{-1} were associated with the asymmetric and symmetric of Si-O-Si, Si-O, and Si-OH bonds, respectively, as seen in Figure 2(a).

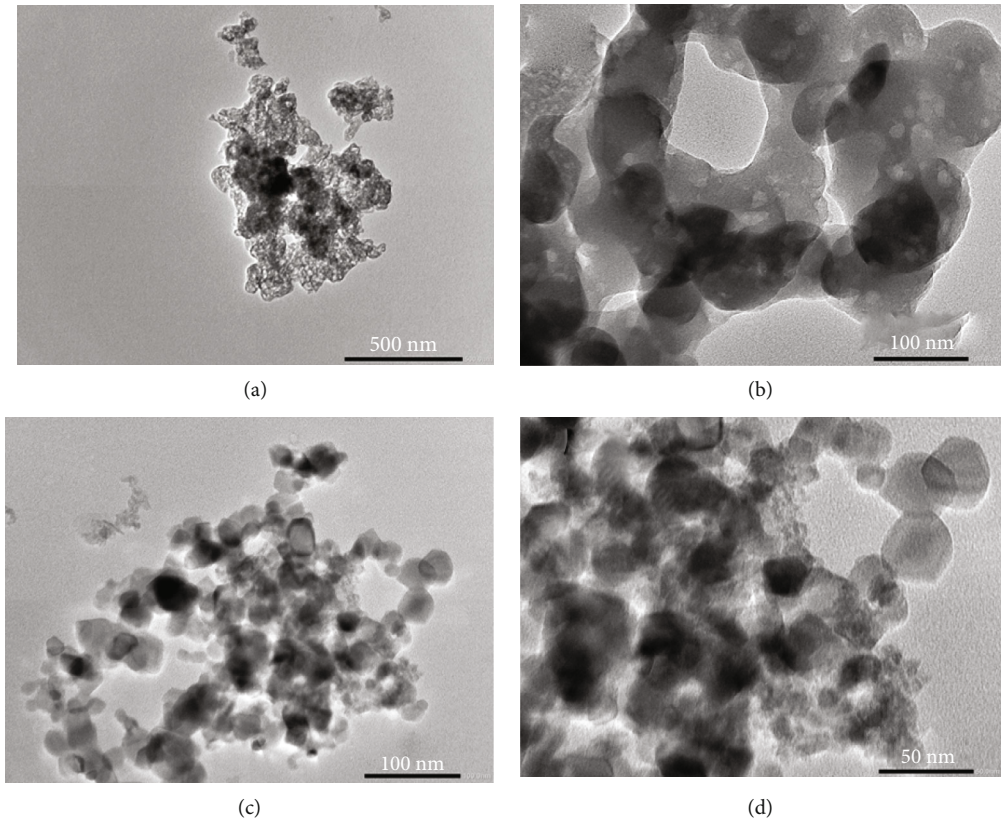

Figure 4: (a, b) TEM images of SiO_2 and (c, d) TEM images of $CuO•Fe_3O_4/SiO_2$ composite.

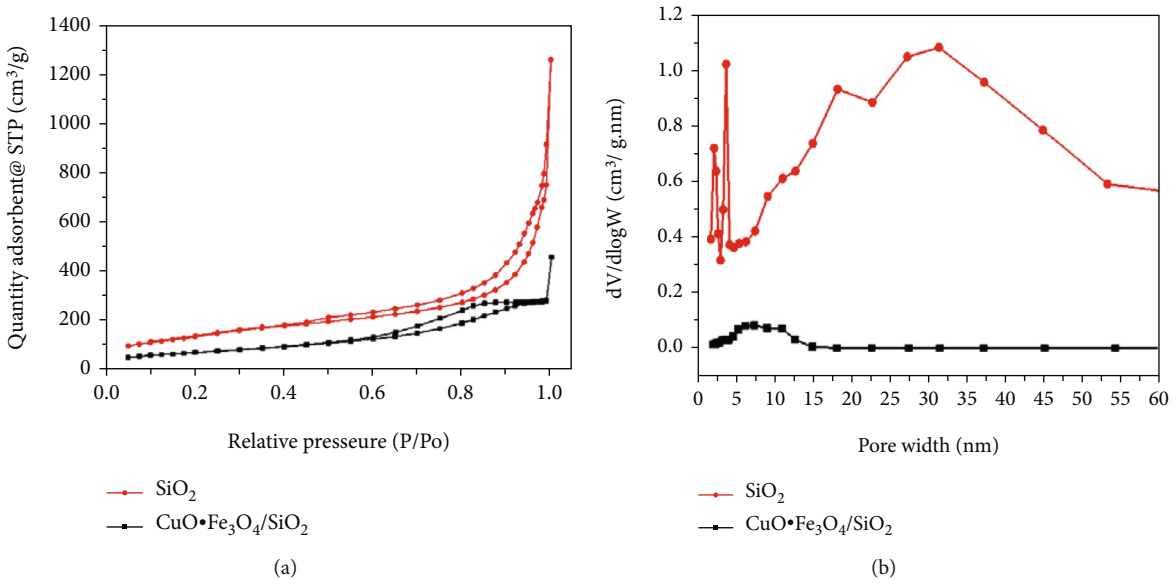

Figure 5: (a) N_2 adsorption/desorption isotherms and (b) pore size distributions of SiO_2 and $CuO•Fe_3O_4/SiO_2$ samples.

The band in 3000–3700 cm^{-1} of the composite was split into two peaks, which shifted to a smaller wave number. The intense bands at 983 and 717 cm^{-1} came from Si-O-Si vibration. In addition, the bands at 484 and 424 cm^{-1} could be assigned to vibrations of Si-Cu-O and Si-Fe-O, respectively, as seen in Figure 2(b), which confirmed that SiO_2 is indeed bound with CuO and Fe_3O_4.

Figure 3 FE-SEM images of SiO_2 and the $CuO•Fe_3O_4/SiO_2$ composite. The structure of SiO_2 was observed as resembling clouds; the uniformly sized SiO_2 particles of about 100–200 nm were gathered together to form a porous structure, in Figures 3(a)–3(c). Meanwhile, the arrangement of metal oxide particles was tight in the composite and them being placed in the channels of SiO_2, in Figures 3(d)–3(f).

Table 1: Textural properties of as-synthesized SiO_2 and as-synthesized $CuO•Fe_3O_4/SiO_2$ composite.

Sample	S_{BET} (m^2/g)	Pore volume (cm^3/g)	Average pore size (nm)
SiO_2	496.4	1.154	9.3
$CuO•Fe_3O_4/SiO_2$	248.6	0.420	6.2

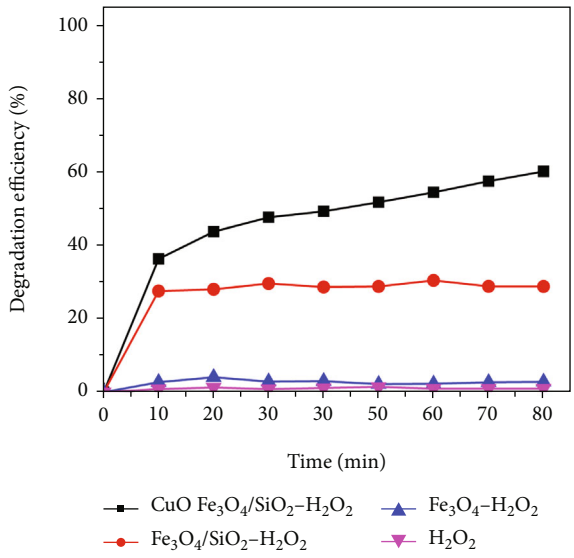

Figure 6: Oxidative degradation of tartrazine in the different catalytic systems. The reaction conditions: dosage catalyst of 0.5 g/L, tartrazine concentration of 50 mg/L, H_2O_2 concentration of 12 mM, and pH = 5.

EDS image and elemental maps indicated that Cu and Fe were evenly dispersed in the composite (Figures 3(g)–3(k), although there was no signal of CuO observed in the XRD (Figure 1).

SiO_2 with a porous structure was observed in the TEM images, in Figures 4(a) and 4(b). There were two types of pores; small pores were formed inside the silica particles after burning the CTAB, and large pores were generated by the arrangement of the silica particles. These could facilitate the dispersion of metal oxide particles on the surface of the silica. As seen in Figures 4(c) and 4(d), the spherical particles of CuO and Fe_3O_4 with a size of about 20–50 nm were uniformly dispersed in the composite. As the result, the porosity and the adsorption capacity of the $CuO•Fe_3O_4/SiO_2$ composite were decreased. However, its catalytic activity was expected to increase due to the presence of metal oxides.

The N_2 adsorption/desorption isotherms of as-prepared samples are shown in Figure 5. It can be observed in Figure 5(a) that the N_2 adsorption/desorption isotherms of SiO_2 and $CuO•Fe_3O_4/SiO_2$ exhibited as the IV isotherm with an H_3 hysteresis loop from the IUPAC classification, indicating the presence of the mesoporous structure in the sample. However, the hysteresis loop of the $CuO•Fe_3O_4/SiO_2$ composite was lowered than that of SiO_2, showing a remarkable reduction in the surface area of the composite; the surface areas were 496.4 m^2/g and 248.6 m^2/g for silica and the composite, respectively. The pore size distribution of SiO_2 was in the range of 2–60 nm, showing the bimodal peak in the range of 2–6 nm and the broad peak in the range of 20–55 nm. This is in complete agreement with the results from the abovementioned TEM. While the large pores ranging from 20–55 nm of the $CuO•Fe_3O_4/SiO_2$ composite disappeared, small pores of the composite remained and its pore size distribution concentrated in the range of 2–15 nm, in Figure 5(b). The average pore sizes of silica and composite were 9.3 and 6.2 nm, and the pore volumes of silica and composite were 1.154 and 0.420 cm^3/g, respectively, in Table 1.

3.2. Degradation of Dyes

3.2.1. The Effect of the Catalytic System. The catalytic activity of the as-prepared samples was examined by the oxidation of TA under reaction conditions: dosage catalyst of 0.5 g/L, TA concentration of 50 mg/L, H_2O_2 concentration of 12 mM, and pH = 5. As indicated in Figure 6, the DE value was only 1% in H_2O_2 within 80 min, which proved that TA was a highly persistent compound and it was difficult to degrade in H_2O_2 even though it was a strong oxidizing agent. The degradation of TA for the Fe_3O_4-H_2O_2 system was also negligible. The DE value increased to 20.1% for the Fe_3O_4/SiO_2-H_2O_2 system and increased to 60.2% for the $CuO•Fe_3O_4/SiO_2$-H_2O_2 system. The porous structure and large specific surface of SiO_2 (Table 1) could facilitate the dispersion of Fe_3O_4, leading to an increase in the catalytic capacity of Fe_3O_4/SiO_2, whereas the simultaneous presence of CuO and Fe_3O_4 oxides on the surface of SiO_2 could enhance the catalytic ability of the $CuO•Fe_3O_4/SiO_2$ composite.

3.2.2. Effect of the Initial pH. The pH in the solution is a vital factor affecting the catalytic removal of dyes in an aqueous solution. It not only affects the surface charge and functional group structure but also affects the rate formation of the $OH^•$ radical. In this study, the effect of pH in the solution on the degradation of TA in the catalytic systems was investigated at the pH in the solution from 3 to 7 under the fixed other conditions; the results are shown in Figure 7. The catalytic performance of the Fe_3O_4-H_2O_2 and F_3O_4/SiO_2-H_2O_2 systems was strongly dependent on the pH in the solution. The DE values of the Fe_3O_4-H_2O_2 and F_3O_4/SiO_2-H_2O_2 systems at pH 3 in 80 min were 98.2 and 85.2%, respectively. The catalytic performance was sharply reduced with the increase of the initial pH. The DE values for the Fe_3O_4-H_2O_2 system were 2.9 and 1.0%; these were 27.2 and 18.7% at pH 5 and 7 for the Fe_3O_4/SiO_2-H_2O_2 system, respectively, in Figures 7(a) and 7(b). These results were consistent with previous studies; the Fenton catalyst of iron oxides showed to be effective at an acidic environment (pH 3–4) [59, 60]. Meanwhile, the degradation of TA in the $CuO•Fe_3O_4/SiO_2$-H_2O_2 system was less affected by pH than

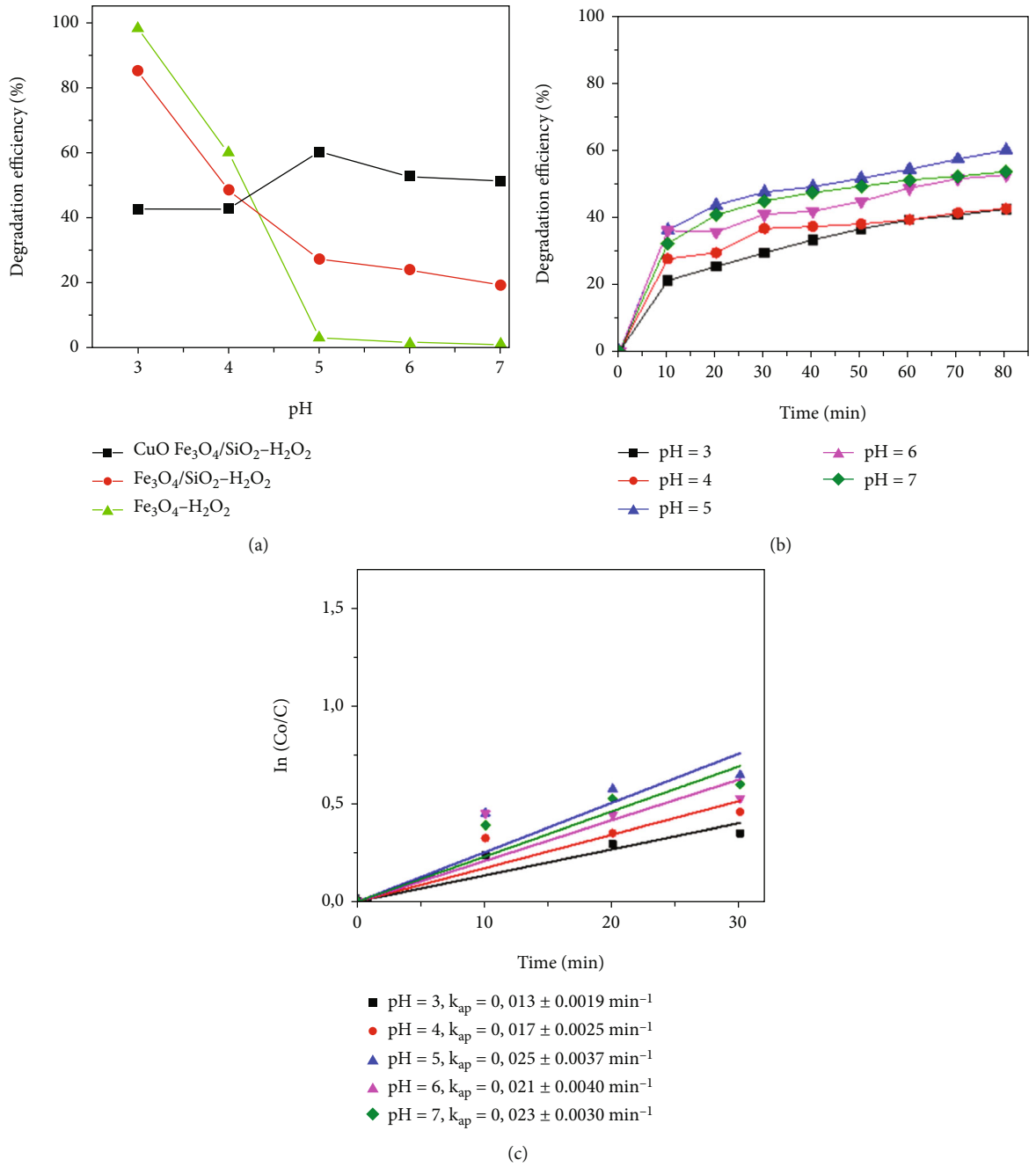

FIGURE 7: (a) Degradation efficiency of tartrazine in the different catalytic systems and pHs, (b) degradation of tartrazine in CuO•Fe_3O_4/SiO_2 at the different initial pHs, and (c) fitting plots.

in the Fe_3O_4-H_2O_2 and F_3O_4/SiO_2-H_2O_2 systems. It could work in a wide pH range from 3 to 7, and the catalytic activity was strongest with a reaction rate of 0.025 min^{-1} at pH 5, in Figure 7(c). The enhancement of catalytic efficiency in the neutral-pH region could be explained by the following reasons: the supporter SiO_2 could expand the pH-active zone of the Fenton catalyst since SiO_2 has multiple hydroxyl groups on the surface. The surrounded –OH groups might chelate with the Fe^{2+} and Fe^{3+} ions to form the weak chelation, benefiting the Fenton reaction at neutral pH [40, 61]. Alternatively, the formation of $[Cu(H_2O)_6]^{2+}$ was concurrent with the generation of $[Fe(H_2O)_6]^{3+}$, which was soluble in the Fenton reaction cycle, which enhanced generating hydroxyl radicals even at high pH [59].

3.2.3. Effect of H_2O_2 Concentration. The effect of the H_2O_2 concentration on the catalytic performance of the CuO•-Fe_3O_4/SiO_2-H_2O_2 system was investigated by increasing the H_2O_2 concentration up to 180 mM at the fixed other conditions (TA concentration of 50 mg/L, dosage catalyst of 0.5 g/L, and pH 5). The degradation efficiency and fitting plots are presented in Figure 8. The absence of H_2O_2 in the

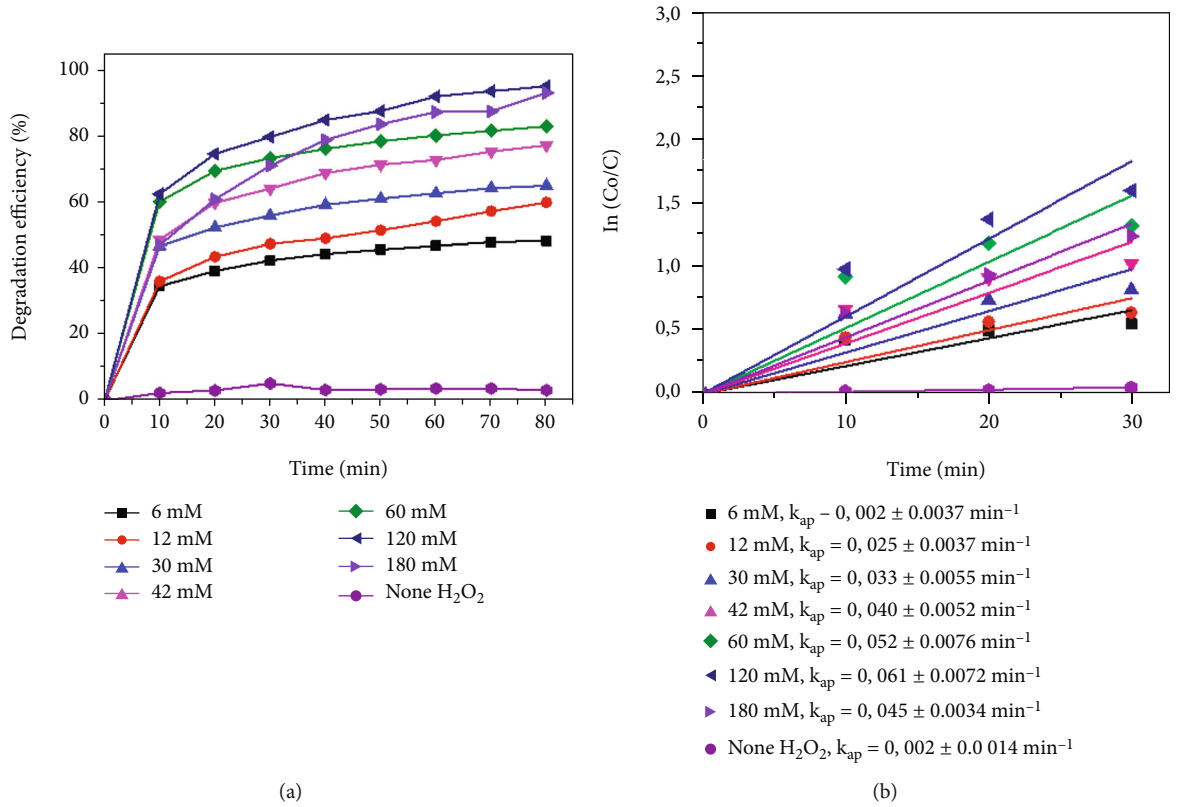

FIGURE 8: (a) Oxidative degradation of tartrazine at the different H_2O_2 concentrations and (b) fitting plots. The reaction conditions: dosage catalyst of 0.5 g/L, tartrazine concentration of 50 mg/L, and pH =5.

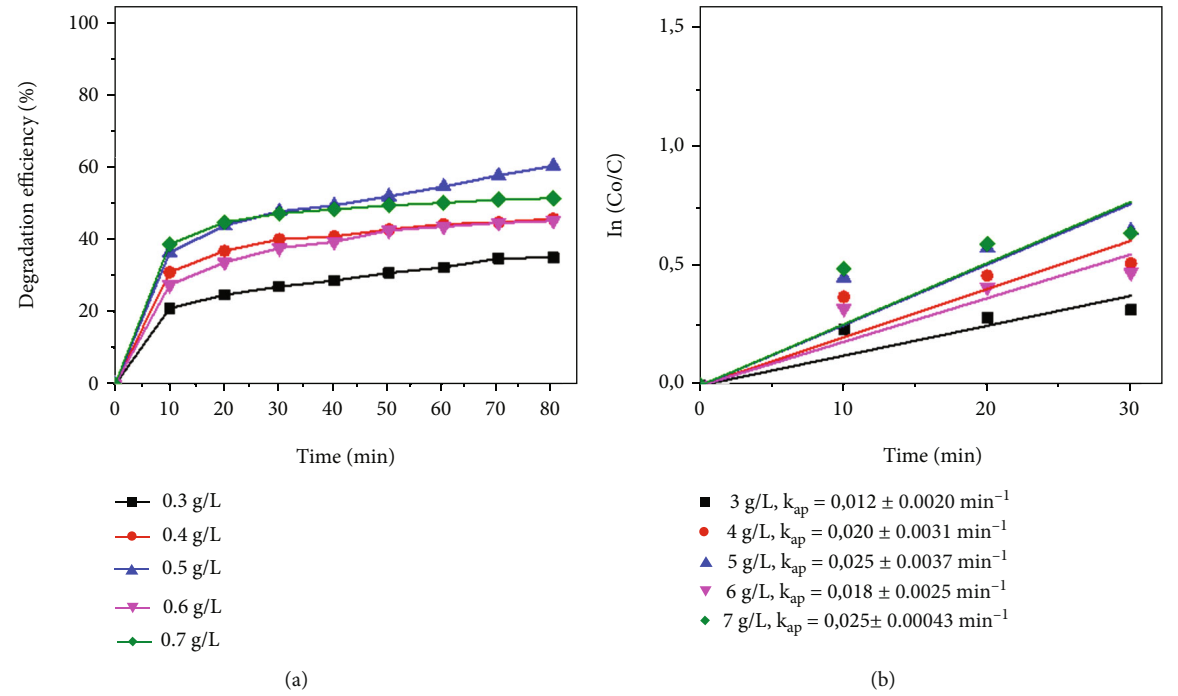

FIGURE 9: (a) Oxidative degradation of tartrazine at the different catalyst dosages and (b) fitting plots. The reaction conditions: tartrazine concentration of 50 mg/L, H_2O_2 concentration of 12 mM, and pH = 5.

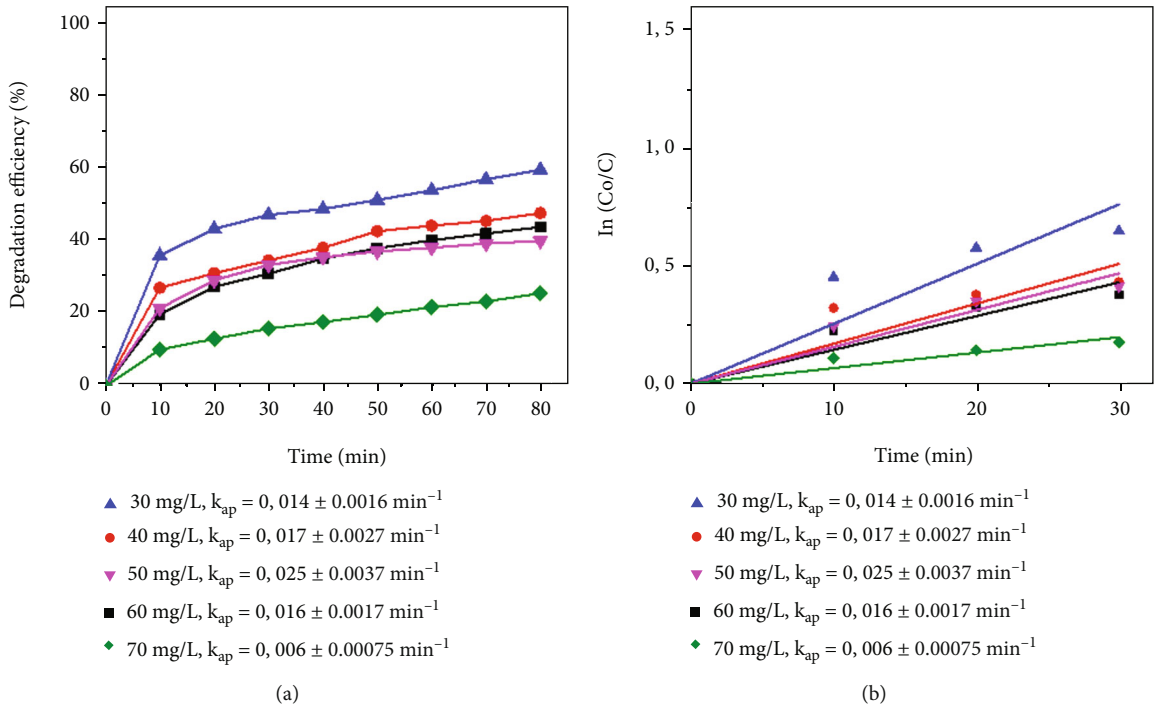

Figure 10: (a) Oxidative degradation of tartrazine at the different concentrations of tartrazine and (b) fitting plots. The reaction conditions: dosage catalyst of 0.5 g/L, H_2O_2 concentration of 12 mM, and pH = 5.

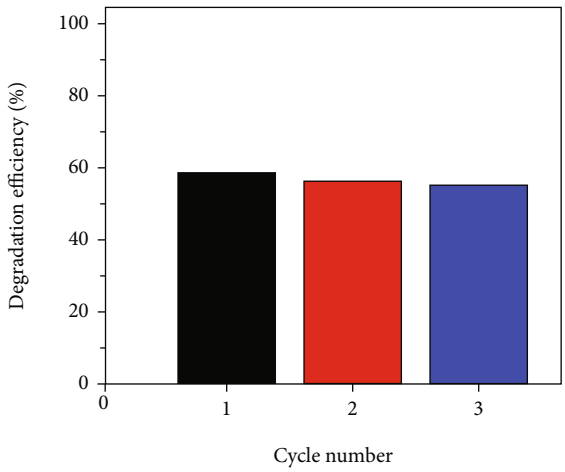

Figure 11: Reusability test of as-synthesized CuO•Fe_3O_4/SiO_2 catalyst. Reaction condition: tartrazine concentration of 50 mg/L, dosage catalyst of 0.5 g/L, H_2O_2 concentration of 12 mM, and pH = 5.

solution led to low the degradation reaction, and the DE and the reaction rate were 3.2% and 0.002 min^{-1}, respectively. These values significantly increased to 48.6% and 0.022 min^{-1}, respectively, in the presence of H_2O_2 at 6 mM. When the concentration of H_2O_2 increased, the DE and reaction rate gradually increased, which achieved 93.3% and 0.061 min^{-1}, respectively, at 120 mM. The increase of the concentration of H_2O_2 could increase rate generation of the hydroxyl radical. However, further increasing the concentration of H_2O_2 to180 mM, the catalytic performance was reduced and the DE and reaction rate were 92% and 0.045 min^{-1}, respectively. When the concentration of H_2O_2 exceeded the critical level, the reaction rate and degradation efficiency decrease since the residual H_2O_2 molecules could act as hydroxyl radical recovery agents; $OH^{\bullet}$ can recombine to form HO_2 and O_2 as expressed in equation (3) [62].

$$H_2O_2 + OH^{\bullet} \longrightarrow HO_2^{\bullet} + H_2O,$$
$$HO_2^{\bullet} + OH^{\bullet} \longrightarrow H_2O + O_2. \quad (3)$$

3.2.4. Effect of the Catalyst Dosage. The effect of the catalyst dosage on photocatalytic performance was studied to determine the optimum amount of photocatalyst added to the catalytic process. In this study, the catalyst dosage varied from 0.3 up to 0.7 g/L under the fixed conditions (TA concentration of 50 mg/L, H_2O_2 concentration of 12 mM, and pH 5); the results are presented in Figure 9. The reaction increased when raising the catalyst dosage from 0.3 to 0.5 g/L, showing the increase of DE within 80 min from 34.9 to 60.1%. However, the reaction was declined at the higher catalyst dosage than 0.5 g/L; the DE values were 44.9 and 51.1% for the catalyst dosages of 0.6 and 0.7 g/L, respectively. The obtained results are related to the number of active sites on the catalyst surface, which increase with the addition of the catalyst, leading to enhanced photocatalytic performance. Meanwhile, the high catalyst concentration (>0.5 g/L) can lead to agglomeration of the reaction sites thereby slowing the TA removal efficiency [63, 64]. In addition, quenching of $OH^{\bullet}$ radials by excess iron ions in the reaction process, equation (4)) [1], may also be

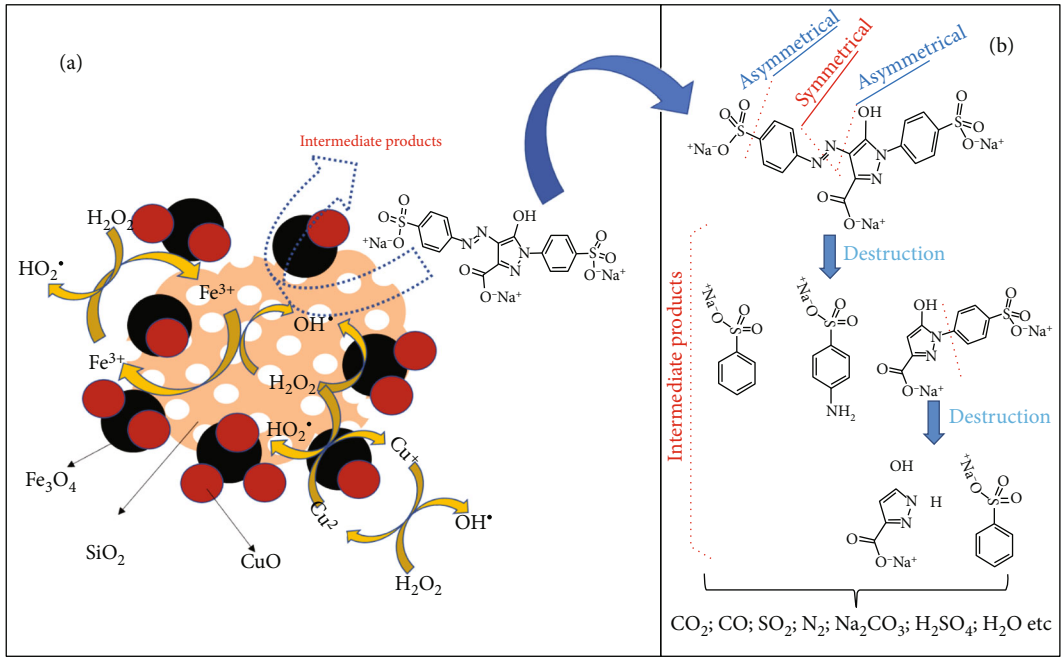

FIGURE 12: (a) The reaction mechanism of tartrazine on the CuO•Fe_3O_4/SiO_2 composite and (b) possible route to the destruction of tartrazine in as-synthesized CuO•Fe_3O_4/H_2O_2 system.

responsible for the result [1].

$$Fe^{2+} + 2OH^{\bullet} \longrightarrow Fe^{3+} + 2OH^{-}. \quad (4)$$

3.2.5. Effect of the Initial Dye Concentration. The influence of the initial dye concentration on the catalytic efficiency of the CuO•Fe_3O_4/SiO_2 composite was demonstrated in the TA concentration range of 30–70 mg/L under fixed conditions (dosage catalyst of 0.5 g/L, H_2O_2 concentration of 12 mM, and pH 5), and the obtained results are presented in Figure 10. It indicated that the optimum TA concentration was 50 mg/L; the DE and reaction rate reached 60.1% and 0.025 min^{-1}, respectively. At lower concentrations, the frequency of collisions between the TA molecules and the catalyst surface was low, leading to a slow reaction [65]. At concentration above 50 mg/L. The degradation efficiency was decreased with an increase in TA concentration. Which could be could be assigned to either the low ratio of [$OH^{\bullet}$]/[TA] at a similar catalyst dosage and H_2O_2 concentration or the block of the interaction of dyes molecules with active sites of the catalyst due to the competition of intermediates generated in the dye degradation process [66].

3.3. Reusability of the Catalyst and Reaction Mechanism Discussion. For a catalyst, reproducibility is one of the important parameters to advance to commercial application. At the end of each experiment, the catalyst was filtered and washed alternately with distilled water and ethanol 2–3 times and then dried in the oven at 80°C for 12 h for the next cycle. The DE slightly decreased after each cyclic experiment. The efficiency of the 3rd reuse was 55.1%, equivalent to 93.5% of the first use, in Figure 11.

The mechanism of oxidative degradation of TA by H_2O_2 in the CuO•Fe_3O_4/SiO_2 catalyst is proposed in Figure 12. Porous SiO_2 acts as a supporter; the good adsorption can increase the interaction between H_2O_2 and the catalyst surface. Therefore, the formation of free radicals occurs rapidly. SiO_2-Fe^{2+}/Fe^{3+} may activate H_2O_2, leading to the formation of hydroxyl ($OH^{\bullet}$) and perhydroxyl ($HO_2^{\bullet}$) radicals according to reaction (5). In addition, the $OH^{\bullet}$ and $HO_2^{\bullet}$ radicals can be created by SiO_2-Cu^{2+} via reaction (6). And, the $OH^{\bullet}$ and $HO_2^{\bullet}$ radicals oxidize TA to form CO_2, H_2O, and other byproducts based on reaction (7). However, $OH^{\bullet}$ plays a significant role in the oxidation of organic pollutants because it has higher oxidation potential than $HO_2^{\bullet}$ [67]. The fragmentation mechanism of TA can be proposed in Figure 12(b) including the cleavage of the symmetrical and asymmetrical azo bonds by the $OH^{\bullet}$ radical [1].

$$\begin{aligned} SiO_2 - Fe^{3+} + H_2O_2 &\longrightarrow SiO_2 - Fe^{2+} + HO_2^{\bullet} + H^{+}, \\ SiO_2 - Fe^{2+} + H_2O_2 &\longrightarrow SiO_2 - Fe^{3+} + OH^{\bullet} + OH^{-}, \end{aligned} \quad (5)$$

$$\begin{aligned} SiO_2 - Cu^{2+} + H_2O_2 &\longrightarrow SiO_2 - Cu^{+} + HO_2^{\bullet} + H^{+}, \\ SiO_2 - Cu^{+} + H_2O_2 &\longrightarrow SiO_2 - Cu^{2+} + OH^{\bullet} + OH^{-}, \end{aligned} \quad (6)$$

$$\frac{OH^{\bullet}}{HO_2^{\bullet}{}_{-}} + TA \longrightarrow \text{intermediate products},$$

$$\frac{OH^{\bullet}}{HO_2^{\bullet}{}_{-}} + \text{intermediate products} \longrightarrow CO_2 + H_2O + \text{byproducts}. \quad (7)$$

Table 2: Comparison of the removal efficiency of the dyes by different catalysts.

Catalyst/adsorbent	Reaction conditions	Observation	Reference
As-synthesized CuO•Fe_3O_4/SiO_2/H_2O_2, Fenton-like catalyst	[cat.] = 0.5 g/L, [H_2O_2] = 12 mM, pH = 5, [TA] = 50 mg/L, T = 30°C	93.3% of dye was removed within 80 min and 55.1% in the third cycle	This work
Fe_2O_3•SiO_2/H_2O_2, Fenton-like catalyst	[cat.] = 0.5 g/L, [H_2O_2] = 12 mM, pH = 3, [TA] = 50 mg/L, T = 30°C	98.5% of dye was removed within 80 min and 86.7% in the third cycle	[1]
Sodium alginate/Fe_3O_4, Fenton-like catalyst	[cat.] = 5 g/L, [H_2O_2] = 100 ppm, pH = 5, [BPA] = 20 ppm, T = 30°C	95% of BPA was removed within 120 min	[69]
Al, Fe-pillared clays, Fenton-like catalyst	[cat.] = 5 g/L, [TA] = 50 mg/L, [H_2O_2] = 0.12 M, T = 75°C	97.5% of dye was removed within 240 min	[70]
Powder-activated carbon/Fe_3O_4, Fenton-like catalyst	[cat.] = 0.3 g/L, pH = 3, [H_2O_2] = 3 mL/L, [metronidazole] = 50 mg/L	96.12% of metronidazole was removed within 90 min	[71]
Fe electrode; electro-Fenton	[H_2O_2] = 0.32 mM/L, [NaCl] = 0.3 mg/L, pH = 3, [diazinon] = 20 ppm, δ = 5.14 mA/cm^2	100% of diazinon was removed within 34.49 min	[72]
SS316/β-PbO_2 anode, electro-Fenton, and sono-electro-Fenton	[$FeSO_4$] = 0.24 g/L, [NaCl] = 0.1 g/L, pH = 5.3 , [H_2O_2] = 30 mg/L, [diazinon] = 45.6 mg/L, voltage = 13.8 V	92% of diazinon was removed; 73.2% of COD and 67.4% of TOC were reduced after 75 min	[73]
SS316/β-PbO_2, Fenton, and electro-Fenton	[$FeSO_4$] = 0.3 g/L, [H_2O_2] = 0.12 mg/L, [oxytetracycline] = 20 mg/L, pH = 3.53, δ = 3.85 mA/cm^2	Oxytetracycline was removed at 84.7%, 73.4%, and 98.2% in electrochemical, Fenton, and electro-Fenton processes, respectively, after 42 min	[74]
3D/SEF/PAC/Fe_3O_4, sono-electro-Fenton	[cat.] = 5 g/L, [H_2O_2] = 0.2 mL/L, [$FeSO_4$] = 0.08 mg/L, [2, 4 − D] = 50 mβL, pH = 3, δ = 5 mA/cm^2, [Na_2SO_4] = 0.3 g/250 mL	96.2% of 2,4-dichlorophenoxyacetic acid was removed, and 92.31% of COD and 86.5% of TOC were reduced after 60 min	[75]
Fe electrode-sodium persulfate, electro-Fenton	[cat.] = 0.09 g/L, [$Na_2S_2O_8$] = 0.9 g/L, [NaCl] = 0.2 g/L, [BV16] = 45 mg/L, pH = 5, U = 11.43 V	95% of dye was removed, and 57.14% of COD was reduced after 48.5 min	[10]
Graphite/β-PbO_2 anode, electrochemical degradation	pH = 5.75, δ = 10 mA/cm^2, [Na_2SO_4] = 78.8 mg/L	96.2% of methylene blue was removed after 50 min	[13]
UVC/$Na_2S_2O_8$/Fe^{2+}	[SPS] = 0.601 mM, $[Fe^{2+}]$ = 0.075 mM, [dimethyl phthalate] = 5 mg/L, pH = 11	97% of dimethyl phthalate was removed, and 64.2% of TOC was reduced within 90 min	[25]
UV/ZnO, photocatalyst	[cat.] = 0.15 g/L, pH = 5, [phenol] = 10 mg/L, UV lamp = 125 W	94.2% of phenol was removed after 30 min	[22]
Au/ZnO/H_2O_2 photocatalyst	[cat.] = 0.5 g/L, [H_2O_2] = 50 mM, pH = 6, [dye] = 10 mg/L, Hg lamp = 250 W	99.2% of dye was removed after 30 min	[76]
Magnetic zeolite nanocomposite (MZNC) (zeolite : Fe_3O_4 = 2 : 1), adsorption	[ads.] = 1 g/L, pH = 3, T = 50°C	96.12% of dimethyl phthalate was removed within 20 min, and the removal efficiency was 70.63% in the tenth cycle	[28]
Magnetic iron oxide/graphene oxide (MGO), adsorption	[ads.] = 0.334 g/L, pH = 5.38, [diethyl phthalate] = 4.241 mg/L	100% of diethyl phthalate was removed within 3.723 min	[29]
GO-Fe_3O_4, adsorption	[ads.] = 0.178 g/L, pH = 4.45, [2, 4 − dinitrophenol] = 50.10 mg/L, ultrasound frequency = 40.02 kHz	89.94% of 2,4-dinitrophenol was adsorbed, and the adsorption of the reuse adsorbent in both systems after 10th consecutive cycles was reduced by about 22%	[30]
Clinoptilolite zeolite/Fe_3O_4 nanoparticles, adsorption	[ads.] = 0.5 g/L, [BV16] = 25 mg/L, pH = 7, mixing speed = 250 rpm	99% of dye was removed after 45 min	[11]
Lignin-containing cellulose (LCNF), adsorption	[ads.] = 0.3 g/L, [Pb] = 10 mg/L, pH = 6, T = 25°C	99% of Pb was removed after 60 min	[77]

In addition, with the appearance of free radicals, Fe^{3+} and Fe^{2+} ions will be regenerated according to equation (8) [1, 36]. However, this process is quite slowly.

$$\begin{aligned} OH^{\bullet} + SiO_2 - Fe^{2+} &\longrightarrow OH^{-} + SiO_2 - Fe^{3+}, \\ HO_2^{\bullet} + SiO_2 - Fe^{2+} &\longrightarrow HO_2^{-} + SiO_2 - Fe^{3+}, \\ HO_2^{\bullet} + SiO_2 - Fe^{3+} &\longrightarrow H^{+} + O_2 + SiO_2 - Fe^{2+}. \end{aligned} \quad (8)$$

On other hand, the standard redox potential value of Fe^{3+}/Fe^{2+} ($E^{\circ} = 0.77$ V) is larger than that of Cu^{2+}/Cu^{+} ($E^{\circ} = 0.17$ V). Therefore, the presence of Cu^{2+}/Cu^{+} will promote the regeneration of Fe^{3+} and Fe^{2+} according to equation (9) [36, 68] as follows:4

$$SiO_2 - Fe^{3+} + SiO_2 - Cu^{+} \longrightarrow SiO_2 - Fe^{2+} + SiO_2 - Cu^{2+}. \quad (9)$$

3.4. Comparison with Other Catalysts. The catalytic performance of the as-prepared $CuO\bullet Fe_3O_4/SiO_2$ composite was compared with other catalysts recently studied on the removal of persistent organic compounds in water such as Fenton [1, 69–71], electro-Fenton [10, 13, 25, 72–75], photocatalyst [22, 76], and adsorption [11, 28–30, 77]. The reaction conditions and decomposition efficiency of these catalysts are listed in Table 2. The removal efficiency is dependent not only on the type of catalyst and the nature of the organic compound but also on the temperature, the stirring rate, the pH of the solution, the reaction time, and the concentration of the reactants. Therefore, direct comparison among catalysts is a challenge but the relative performance of the $CuO\bullet Fe_3O_4/SiO_2$ catalyst can be evaluated indirectly.

In Table 2, in comparison with the catalytic mechanism as a Fenton-like system, the DE of as-prepared $CuO\bullet Fe_3O_4/SiO_2$ was lower but the pH range for reaction occurred was wider than that of Fe_2O_3/SiO_2, sodium alginate/Fe_3O_4, Al, Fe-pillared clays, and powder-activated carbon/Fe_3O_4. The electron-Fenton system using the Fe electrode, SS316/β-PbO_2, 3D/SEF/PAC/Fe_3O_4, Fe electrode-sodium persulfate, and graphite/β-PbO_2 anode had a high degradation rate, but these processes required additional conditions associated with the reaction such as the addition of electrolyte, application of the current, and designing the appropriate electrode. Photocatalysts based on ZnO or Au/ZnO have a faster degradation rate of tartrazine than $CuO\bullet Fe_3O_4/SiO_2$, but the oxidation reaction took place at a low dye concentration, 10 mg/L. Adsorbents of GO-Fe_3O_4, magnetic zeolite nanocomposite, clinoptilolite zeolite/Fe_3O_4 nanoparticles, and lignin-containing cellulose had relatively high removal of organic compounds, but their poor reuse was a limitation for these materials. Therefore, the $CuO\bullet Fe_3O_4/SiO_2$ composite prepared by the simple coprecipitation method is expected to reduce the cost of the catalyst for large-scale application.

4. Conclusion

Mesoporous SiO_2 was successfully prepared from RH with the assistance of CTAB. Silica had an amorphous structure with a relatively large surface area of 496.4 m^2/g and a relatively high pore volume of 1.154 cm^3/g. The $CuO\bullet Fe_3O_4/SiO_2$ composite was successfully prepared from obtained silica by a simple coprecipitation method for oxidizing dye. Metal oxide particles, Fe_3O_4 and CuO, of poor crystallinity and spherical shape with a particle size of approximately 20–50 nm, were well dispersed on the porous structure of SiO_2. These could reduce the textural values of the $CuO\bullet Fe_3O_4/SiO_2$ composite; the surface area, pore volume, and average pore size of the composite were 248.6 m^2/g, 0.420 cm^3/g, and 6.2 nm, respectively.

The effects of reaction conditions such as catalyst dosage and initial dye concentration on the catalytic performance of the composite were studied. The reusability of the catalyst was investigated by cyclic experiments. The adsorption ability of the composite was decreased; however, the catalytic efficiency of the composite for oxidizing dye could be enhanced. The degradation of TA for the Fe_3O_4-H_2O_2 system was also negligible. The DE was increased to 60.2% for the $CuO\bullet Fe_3O_4/SiO_2$-H_2O_2 system. Porous SiO_2 acted as a supporter; the good adsorption could increase the interaction between H_2O_2 and the catalyst surface. Therefore, the formation of free radicals occurred rapidly. The SiO_2-Fe^{2+}/Fe^{3+} from Fe_3O_4 might activate H_2O_2 leading to the formation of hydroxyl ($OH^{\bullet}$) and perhydroxyl ($HO_2^{\bullet}$) radicals. In addition, the presence of Cu^{2+}/Cu^{+} could promote the regeneration of Fe^{3+} and Fe^{2+}. As the result, the catalytic efficiency of $CuO\bullet Fe_3O_4/SiO_2$ could be enhanced in the wide pH range of 3–7.

Data Availability

The research data used to support the findings of this study are included within the article.

Conflicts of Interest

The authors declare that they have no conflicts of interest.

Acknowledgments

The authors are grateful for the financial support from the Vietnam National Foundation for Science and Technology Development (NAFOSTED) under grant number 104.05-2018.333.

References

[1] A. T. Vu, T. N. Xuan, and C. H. Lee, "Preparation of mesoporous Fe_2O_3*SiO_2 composite from rice husk as an efficient heterogeneous Fenton-like catalyst for degradation of organic dyes," *Journal of Water Process Engineering*, vol. 28, pp. 169–180, 2019.

[2] T. Nguyen and B. Singh, "Trend in Rice Production and Export in Vietnam," *Omonrice*, vol. 14, pp. 111–123, 2006.

[3] A. T. Vu, T. A. Tuyet Pham, T. T. Tran et al., "Synthesis of nano-flakes Ag•ZnO•activated carbon composite from rice husk as a photocatalyst under solar light," *Bulletin of Chemical Reaction Engineering & Catalysis*, vol. 15, no. 1, pp. 264–279, 2020.

[4] O. Mohiuddin, A. Mohiuddin, M. Obaidullah, H. Ahmed, and S. Asumadu-Sarkodie, "Electricity production potential and social benefits from rice husk, a case study in Pakistan," *Cogent Engineering*, vol. 3, no. 1, p. 1177156, 2016.

[5] H. T. Thu, L. T. Dat, and V. A. Tuan, "Synthesis of mesoporous SiO2from rice husk for removal of organic dyes in aqueous solution," *Vietnam Journal of Chemistry*, vol. 57, no. 2, pp. 175–181, 2019.

[6] R. A. Bakar, R. Yahya, and S. N. Gan, "Production of high purity amorphous silica from rice husk," *Procedia Chemistry*, vol. 19, pp. 189–195, 2016.

[7] S.-S. Huang, M. T. Tung, C. D. Huynh et al., "Engineering rice husk into a high-performance electrode material through an ecofriendly process and assessing its application for lithium-ion sulfur batteries," *ACS Sustainable Chemistry & Engineering*, vol. 7, no. 8, pp. 7851–7861, 2019.

[8] Z. Salahshoor and A. Shahbazi, "Review of the Use of Mesoporous Silicas for Removing Dye from Textile Wastewater," *European Journal of Environmental Sciences*, vol. 4, no. 2, pp. 116–130, 2014.

[9] M. Li, J. T. Li, and H. W. Sun, "Sonochemical decolorization of acid black 210 in the presence of exfoliated graphite," *Ultrasonics Sonochemistry*, vol. 15, no. 1, pp. 37–42, 2008.

[10] K. Hasani, M. Moradi, S. A. Mokhtari, A. Dargahi, and M. Vosoughi, "Degradation of basic violet 16 dye by electro-activated persulfate process from aqueous solutions and toxicity assessment using microorganisms: determination of by-products, reaction kinetic and optimization using Box–Behnken design," *International Journal of Chemical Reactor Engineering*, vol. 19, no. 3, pp. 261–275, 2021.

[11] A. Peyghami, A. Moharrami, Y. Rashtbari, S. Afshin, M. Vosuoghi, and A. Dargahi, "Evaluation of the efficiency of magnetized clinoptilolite zeolite with Fe3O4nanoparticles on the removal of basic violet 16 (BV16) dye from aqueous solutions," *Journal of Dispersion Science and Technology*, vol. 42, pp. 1–10, 2021.

[12] H. Rezaei, M. Haghshenasfard, and A. Moheb, "Optimization of dye adsorption using Fe_3O_4 nanoparticles encapsulated with alginate beads by Taguchi method," *Adsorption Science & Technology*, vol. 35, no. 1-2, pp. 55–71, 2017.

[13] M. R. Samarghandi, A. Dargahi, A. Shabanloo, H. Z. Nasab, Y. Vaziri, and A. Ansari, "Electrochemical degradation of methylene blue dye using a graphite doped PbO_2 anode: optimization of operational parameters, degradation pathway and improving the biodegradability of textile wastewater," *Arabian Journal of Chemistry*, vol. 13, no. 8, pp. 6847–6864, 2020.

[14] M. A. Alaei Shahmirzadi, S. S. Hosseini, J. Luo, and I. Ortiz, "Significance, evolution and recent advances in adsorption technology, materials and processes for desalination, water softening and salt removal," *Journal of Environmental Management*, vol. 215, pp. 324–344, 2018.

[15] G. M. Klecka, S. J. Gonsior, R. J. West, P. A. Goodwin, and D. A. Markham, "Biodegradation of bisphenol a in aquatic environments: river die-away," *Environmental Toxicology and Chemistry: An International Journal*, vol. 20, no. 12, pp. 2725–2735, 2001.

[16] A. D. Bokare and W. Choi, "Review of iron-free Fenton-like systems for activating H_2O_2 in advanced oxidation processes," *Journal of Hazardous Materials*, vol. 275, pp. 121–135, 2014.

[17] X. Tang, Q. Feng, K. Liu, Z. Li, and H. Wang, "Fabrication of magnetic Fe_3O_4/silica nanofiber composites with enhanced Fenton-like catalytic performance for Rhodamine B degradation," *Journal of Materials Science*, vol. 53, no. 1, pp. 369–384, 2018.

[18] X. Tang, Z. Li, K. Liu et al., "Sulfidation modified Fe_3O_4 nanoparticles as an efficient Fenton-like catalyst for azo dyes degradation at wide pH range," *Powder Technology*, vol. 376, pp. 42–51, 2020.

[19] K. Rovina, S. Siddiquee, and S. M. Shaarani, "A review of extraction and analytical methods for the determination of tartrazine (E 102) in foodstuffs," *Critical Reviews in Analytical Chemistry*, vol. 47, no. 4, pp. 309–324, 2017.

[20] EFSA Panel on Food Additives and Nutrient Sources Added to Food, "Scientific Opinion on the re-evaluation Tartrazine (E 102)," *EFSA Journal*, vol. 7, no. 11, article 1331, 2009.

[21] F. I. de Andrade, M. I. F. Guedes, Í. G. P. Vieira et al., "Determination of synthetic food dyes in commercial soft drinks by TLC and ion-pair HPLC," *Food Chemistry*, vol. 157, pp. 193–198, 2014.

[22] D. J. Naghan, A. Azari, N. Mirzaei et al., "Parameters effecting on photocatalytic degradation of the phenol from aqueous solutions in the presence of ZnO nanocatalyst under irradiation of UV-C light," *Bulgarian Chemical Communications*, vol. 47, pp. 14–18, 2016.

[23] M. R. Samarghandi, A. Dargahi, H. Zolghadr Nasab, E. Ghahramani, and S. Salehi, "Degradation of azo dye Acid Red 14 (AR14) from aqueous solution using H_2O_2/nZVI and $S_2O_8^{2-}$/nZVI processes in the presence of UV irradiation," *Water Environment Research*, vol. 92, no. 8, pp. 1173–1183, 2020.

[24] A. Seid-Mohammadi, Z. Ghorbanian, G. Asgari, and A. Dargahi, "Photocatalytic degradation of metronidazole (MnZ) antibiotic in aqueous media using copper oxide nanoparticles activated by H_2O_2/UV process: biodegradability and kinetic studies," *Desalin. Water Treat*, vol. 193, pp. 369–380, 2020.

[25] M. Y. Badi, A. Esrafili, H. Pasalari et al., "Degradation of dimethyl phthalate using persulfate activated by UV and ferrous ions: optimizing operational parameters mechanism and pathway," *Journal of Environmental Health Science & Engineering*, vol. 17, no. 2, pp. 685–700, 2019.

[26] A. Seidmohammadi, G. Asgari, A. Dargahi et al., "A comparative study for the removal of methylene blue dye from aqueous solution by novel activated carbon based adsorbents," *Progress in Color, Colorants and Coatings*, vol. 12, no. 3, pp. 133–144, 2019.

[27] A. Azari, A. A. Babaie, R. Rezaei-Kalantary, A. Esrafili, M. Moazzen, and B. Kakavandi, "Nitrate removal from aqueous solution by carbon nanotubes magnetized with nano zero-valent iron," *Journal of Mazandaran University of Medical Sciences*, vol. 23, no. 2, pp. 15–27, 2014.

[28] E. Ahmadi, B. Kakavandi, A. Azari et al., "The performance of mesoporous magnetite zeolite nanocomposite in removing dimethyl phthalate from aquatic environments," *Desalination and Water Treatment*, vol. 57, no. 57, pp. 1–15, 2016.

[29] A. Azari, M. H. Mahmoudian, M. H. Niari et al., "Rapid and efficient ultrasonic assisted adsorption of diethyl phthalate onto $Fe^{II}Fe_2{}^{III}O_4$@GO: ANN-GA and RSM-DF modeling,

isotherm, kinetic and mechanism study," *Microchemical Journal*, vol. 150, p. 104144, 2019.

[30] A. Azari, M. Yeganeh, M. Gholami, and M. Salari, "The superior adsorption capacity of 2,4-dinitrophenol under ultrasound- assisted magnetic adsorption system: Modeling and process optimization by central composite design," *Journal of Hazardous Materials*, vol. 418, p. 126348, 2021.

[31] R. RezaeiKalantary, A. JonidiJafari, B. Kakavandi, S. Nasseri, A. Ameri, and A. Azari, "Adsorption and magnetic separation of lead from synthetic wastewater using carbon/iron oxide nanoparticles composite," *Journal of Mazandaran University of Medical Sciences*, vol. 24, no. 113, pp. 172–183, 2014.

[32] S. Y. Hashemi, A. Azari, M. Raeesi, and K. Yaghmaeian, "Application of response surface methodology (RSM) in optimisation of fluoride removal by magnetic chitosan/graphene oxide composite: kinetics and isotherm study," *International Journal of Environmental Analytical Chemistry*, vol. 101, pp. 1–19, 2021.

[33] A. Dargahi, M. Pirsaheb, S. Hazrati, M. Fazlzadehdavil, R. Khamutian, and T. Amirian, "Evaluating efficiency of H_2O_2 on removal of organic matter from drinking water," *Desalination and Water Treatment*, vol. 54, no. 6, pp. 1589–1593, 2014.

[34] A. Seid-Mohammadi, G. Asgarai, Z. Ghorbanian, and A. Dargahi, "The removal of cephalexin antibiotic in aqueous solutions by ultrasonic waves/hydrogen peroxide/nickel oxide nanoparticles (US/H_2O_2/NiO) hybrid process," *Separation Science and Technology*, vol. 55, no. 8, pp. 1558–1568, 2020.

[35] N. Christensen, D. J. Batstone, Z. He, I. Angelidaki, and J. E. Schmidt, "Removal of polycyclic aromatic hydrocarbons (PAHs) from sewage sludge by anaerobic degradation," *Water Science and Technology: a Journal of the International Association on Water Pollution Research*, vol. 50, no. 9, pp. 237–244, 2004.

[36] V. T. Le, V. D. Doan, V. A. Tran et al., "Cu/Fe_3O_4@carboxylate-rich carbon composite: one-pot synthesis, characterization, adsorption and photo-Fenton catalytic activities," *Materials Research Bulletin*, vol. 129, p. 110913, 2020.

[37] M. M. Bello and A. A. A. Raman, "Synergy of adsorption and advanced oxidation processes in recalcitrant wastewater treatment," *Environmental Chemistry Letters*, vol. 17, no. 2, pp. 1125–1142, 2019.

[38] T. V. Anh, T. A. T. Pham, V. H. Mac, and T. H. Nguyen, "Facile controlling of the physical properties of zinc oxide and its application to enhanced photocatalysis," *Journal of Analytical Methods in Chemistry*, vol. 2021, Article ID 5533734, 12 pages, 2021.

[39] T. A. T. Pham, V. A. Tran, V. D. Le et al., "Facile preparation of ZnO nanoparticles and ag/ZnO nanocomposite and their photocatalytic activities under visible light," *International Journal of Photoenergy*, vol. 2020, Article ID 8897667, 14 pages, 2020.

[40] X. Liu, C. Sun, L. Chen et al., "Decoloration of methylene blue by heterogeneous Fenton-like oxidation on Fe_3O_4/SiO_2/C nanospheres in neutral environment," *Materials Chemistry and Physics*, vol. 213, pp. 231–238, 2018.

[41] S. Mandal, S. Adhikari, S. Pu, X. Wang, D.-H. Kim, and R. K. Patel, "Interactive Fe_2O_3/porous SiO_2 nanospheres for photocatalytic degradation of organic pollutants: kinetic and mechanistic approach," *Chemosphere*, vol. 234, pp. 596–607, 2019.

[42] L. Liu, S. Liu, S. B. Mishra, and L. Sheng, "Iron-included mesoporous silica thin slice as adsorbent and Fenton-like catalyst for the adsorption and degradation of dye in wastewater," *Ceramics International*, vol. 45, no. 12, pp. 15475–15481, 2019.

[43] Z. Wu, W. Zhu, M. Zhang et al., "Adsorption and synergetic Fenton-like degradation of methylene blue by a novel mesoporous α-Fe2O3/SiO2at neutral pH," *Industrial & Engineering Chemistry Research*, vol. 57, no. 16, pp. 5539–5549, 2018.

[44] Z. Mao, Q. Wu, M. Wang, Y. Yang, J. Long, and X. Chen, "Tunable synthesis of SiO2-encapsulated zero-valent iron nanoparticles for degradation of organic dyes," *Nanoscale Research Letters*, vol. 9, no. 1, article 501, 2014.

[45] R. Huang, Z. Fang, X. Fang, and E. P. Tsang, "Ultrasonic Fenton-like catalytic degradation of bisphenol A by ferroferric oxide (Fe_3O_4) nanoparticles prepared from steel pickling waste liquor," *Journal of Colloid and Interface Science*, vol. 436, pp. 258–266, 2014.

[46] B. Kakavandi, N. Bahari, R. R. Kalantary, and E. D. Fard, "Enhanced sono-photocatalysis of tetracycline antibiotic using TiO_2 decorated on magnetic activated carbon (MAC@ T) coupled with US and UV: a new hybrid system," *Ultrasonics Sonochemistry*, vol. 55, pp. 75–85, 2019.

[47] S. Zhang, Q. Fan, H. Gao et al., "Formation of Fe_3O_4@MnO_2 ball-in-ball hollow spheres as a high performance catalyst with enhanced catalytic performances," *Journal of Materials Chemistry A*, vol. 4, no. 4, pp. 1414–1422, 2016.

[48] A. Peyghami, A. Moharrami, Y. Rashtbari, S. Afshin, M. Vosuoghi, and A. Dargahi, "Evaluation of the efficiency of magnetized clinoptilolite zeolite with Fe_3O_4 nanoparticles on the removal of basic violet 16 (BV16) dye from aqueous solutions," *Journal of Dispersion Science and Technology*, vol. 42, pp. 1–10, 2021.

[49] H. Ghasemi, S. Mozaffari, S. H. Mousavi, B. Aghabarari, and N. Abu-Zahra, "Decolorization of wastewater by heterogeneous Fenton reaction using MnO_2-Fe_3O_4/CuO hybrid catalysts," *Journal of Environmental Chemical Engineering*, vol. 9, no. 2, p. 105091, 2021.

[50] R. Li, P. Zhang, Y. Huang, P. Zhang, H. Zhong, and Q. Chen, "Pd–Fe_3O_4@C hybrid nanoparticles: preparation, characterization, and their high catalytic activity toward Suzuki coupling reactions," *Journal of Materials Chemistry*, vol. 22, no. 42, pp. 22750–22755, 2012.

[51] H. Liang, H. Niu, P. Li et al., "Multifunctional Fe_3O_4@C@Ag hybrid nanoparticles: Aqueous solution preparation, characterization and photocatalytic activity," *Materials Research Bulletin*, vol. 48, no. 7, pp. 2415–2419, 2013.

[52] F. H. Lin and R. A. Doong, "Bifunctional Au– Fe_3O_4 heterostructures for magnetically recyclable catalysis of nitrophenol reduction," *The Journal of Physical Chemistry C*, vol. 115, no. 14, pp. 6591–6598, 2011.

[53] Y. Ding, C. Pan, X. Peng et al., "Deep mineralization of bisphenol A by catalytic peroxymonosulfate activation with nano CuO/Fe_3O_4 with strong Cu-Fe interaction," *Chemical Engineering Journal*, vol. 384, p. 123378, 2020.

[54] J. Liu, Z. Zhao, P. Shao, and F. Cui, "Activation of peroxymonosulfate with magnetic Fe_3O_4–MnO_2 core–shell nanocomposites for 4-chlorophenol degradation," *Chemical Engineering Journal*, vol. 262, pp. 854–861, 2015.

[55] L. Xu and J. Wang, "Magnetic nanoscaled Fe_3O_4/CeO_2 composite as an efficient Fenton-like heterogeneous catalyst for degradation of 4-chlorophenol," *Environmental Science & Technology*, vol. 46, no. 18, pp. 10145–10153, 2012.

[56] H. T. Thu, L. T. Dat, and V. A. Tuan, "Synthesis of mesoporous SiO_2 from rice husk for removal of organic dyes in aqueous solution," *Vietnam Journal of Chemistry*, vol. 57, no. 2, pp. 175–181, 2019.

[57] A. T. Vu, S. Jiang, K. Ho, J. B. Lee, and C. H. Lee, "Mesoporous magnesium oxide and its composites: preparation, characterization, and removal of 2-chloroethyl ethyl sulfide," vol. 269, pp. 82–93, 2015.

[58] J. Ji, P. Zeng, S. Ji, W. Yang, H. Liu, and Y. Li, "Catalytic activity of core-shell structured $Cu/Fe_3O_4@SiO_2$ microsphere catalysts," *Catalysis Today*, vol. 158, no. 3-4, pp. 305–309, 2010.

[59] H. Ghasemi, B. Aghabarari, M. Alizadeh, A. Khanlarkhani, and N. Abu-Zahra, "High efficiency decolorization of wastewater by Fenton catalyst: magnetic iron-copper hybrid oxides," *Journal of Water Process Engineering*, vol. 37, p. 101540, 2020.

[60] L. Xu and J. Wang, "Fenton-like degradation of 2,4-dichlorophenol using Fe_3O_4 magnetic nanoparticles," *Applied Catalysis B: Environmental*, vol. 123-124, pp. 117–126, 2012.

[61] N. A. Zubir, C. Yacou, J. Motuzas, X. Zhang, X. S. Zhao, and J. C. D. da Costa, "The sacrificial role of graphene oxide in stabilising a Fenton-like catalyst GO–Fe 3 O 4," *Chemical Communications*, vol. 51, no. 45, pp. 9291–9293, 2015.

[62] J. Liu, Y. Du, W. Sun, Q. Chang, and C. Peng, "Preparation of new adsorbent-supported Fe/Ni particles for the removal of crystal violet and methylene blue by a heterogeneous Fenton-like reaction," *RSC Advances*, vol. 9, no. 39, pp. 22513–22522, 2019.

[63] A. Takdastan, B. Kakavandi, M. Azizi, and M. Golshan, "Efficient activation of peroxymonosulfate by using ferroferric oxide supported on carbon/UV/US system: a new approach into catalytic degradation of bisphenol A," *Chemical Engineering Journal*, vol. 331, pp. 729–743, 2018.

[64] Z. Wan and J. Wang, "Degradation of sulfamethazine using Fe_3O_4-Mn_3O_4/reduced graphene oxide hybrid as Fenton-like catalyst," *Journal of Hazardous Materials*, vol. 324, pp. 653–664, 2017.

[65] V. T. Le, V. A. Tran, D. L. Tran, T. L. H. Nguyen, and V.-D. Doan, "Fabrication of Fe_3O_4/ composite from MOF-based materials as an efficient and magnetically separable photocatalyst for degradation of ciprofloxacin antibiotic," *Chemosphere*, vol. 270, p. 129417, 2021.

[66] A. Chen, X. Ma, and H. Sun, "Decolorization of KN-R catalyzed by Fe-containing Y and ZSM-5 zeolites," *Journal of Hazardous Materials*, vol. 156, no. 1-3, pp. 568–575, 2008.

[67] L. Singh, P. Rekha, and S. Chand, "Cu-impregnated zeolite Y as highly active and stable heterogeneous Fenton-like catalyst for degradation of Congo red dye," *Separation and Purification Technology*, vol. 170, pp. 321–336, 2016.

[68] Q. C. Do, D.-G. Kim, and S.-O. Ko, "Catalytic activity enhancement of a $Fe_3O_4@SiO_2$ yolk-shell structure for oxidative degradation of acetaminophen by decoration with copper," *Journal of Cleaner Production*, vol. 172, pp. 1243–1253, 2018.

[69] R. Shokoohi, R. Gillani, M. Molla Mahmoudi, and A. Dargahi, "Investigation of the efficiency of heterogeneous Fenton-like process using modified magnetic nanoparticles with sodium alginate in removing bisphenol A from aquatic environments: kinetic studies," *Desalination and Water Treatment*, vol. 101, pp. 185–192, 2018.

[70] P. Banković, A. Milutinović-Nikolić, Z. Mojović et al., "Al,Fe-pillared clays in catalytic decolorization of aqueous tartrazine solutions," *Applied Clay Science*, vol. 58, pp. 73–78, 2012.

[71] A. Seidmohammadi, Y. Vaziri, A. Dargahi, and H. Z. Nasab, "Improved Degradation of Metronidazole in a Heterogeneous Photo-Fenton Oxidation System with PAC/Fe_3O_4 Magnetic Catalyst: Biodegradability, Catalyst Specifications, Process Optimization, and Degradation Pathway," *Biomass Conversion and Biorefinery*, vol. 11, pp. 1–17, 2021.

[72] M. Heidari, M. Vosoughi, H. Sadeghi, A. Dargahi, and S. A. Mokhtari, "Degradation of diazinon from aqueous solutions by electro-Fenton process: effect of operating parameters, intermediate identification, degradation pathway, and optimization using response surface methodology (RSM)," *Separation Science and Technology*, vol. 56, no. 13, pp. 2287–2299, 2021.

[73] A. Dargahi, M. Moradi, R. Marafat et al., "Applications of Advanced Oxidation Processes (Electro-Fenton and Sono-Electro-Fenton) for Degradation of Diazinon Insecticide from Aqueous Solutions: Optimization and Modeling Using RSM-CCD, Influencing Factors, Evaluation of Toxicity, and Degradation Pathway," *Biomass Conversion and Biorefinery*, vol. 11, pp. 1–18, 2021.

[74] K. Hasani, S. Hosseini, H. Gholizadeh, A. Dargahi, and M. Vosoughi, "Enhancing the Efficiency of Electrochemical, Fenton, and Electro-Fenton Processes Using SS316 and SS316/β-PbO_2 Anodes to Remove Oxytetracycline Antibiotic from Aquatic Environments," *Biomass Conversion and Biorefinery*, vol. 11, pp. 1–18, 2021.

[75] A. Dargahi, K. Hasani, S. A. Mokhtari, M. Vosoughi, M. Moradi, and Y. Vaziri, "Highly effective degradation of 2,4-dichlorophenoxyacetic acid herbicide in a three-dimensional sono-electro-Fenton (3D/SEF) system using powder activated carbon (PAC)/Fe_3O_4 as magnetic particle electrode," *Journal of Environmental Chemical Engineering*, vol. 9, no. 5, p. 105889, 2021.

[76] A.-T. Vu, T. A. T. Pham, X. T. Do et al., "Preparation of hierarchical structure au/ZnO composite for enhanced photocatalytic performance: characterization, effects of reaction parameters, and oxidizing agent investigations," *Adsorption Science & Technology*, vol. 2021, article 5201497, 19 pages, 2021.

[77] S. Rastgar, H. Reaei, and H. Yousefi, "Removal of Lead (Pb) from aqueous solutions using lignocellulose nanofiber," *Avicenna Journal of Environmental Health Engineering*, vol. 8, no. 1, pp. 1–8, 2021.